Coastal Engineering 47 (2003) 431–441

Coastal Engineering
An International Journal for Coastal, Harbour and Offshore Engineers

www.elsevier.com/locate/coastaleng

The wave plus current flow over vortex ripples at an arbitrary angle

Ken Haste Andersen[a,*], Carla Faraci[b]

[a] Department of Mechanical Engineering, Technical University of Denmark, Building 115, DK-2800 Kgs., Lyngby, Denmark
[b] Department of Civil and Environmental Engineering, University of Catania, v.le A. Doria 6, 95125 Catania, Italy

Received 4 October 2001; received in revised form 9 October 2002; accepted 8 November 2002

Abstract

This work concerns the wave plus current flow over a sand bed covered by vortex ripples, with the current and the waves coming from different angles. Experiments were performed in a basin, where current and waves were perpendicular, in order to determine the conditions (current strength) leading to a regular ripple pattern formation. Numerical simulations were conducted changing the direction between the waves and the current from 0° to 90° and the ratio between the current strength and the wave orbital velocity from 0.2 to 1.5. Close to the bed, the current aligns parallel to the ripple crests, leading to a veering current profile with the vertical coordinate. The current-related friction coefficient was calculated. It was found that it decreases as the angle approaches 90°, while it increases for decreasing values of the current with a trend that can be described by a power law.

Keywords: Wave; Current; Friction

1. Introduction

To simulate the large-scale flow in the coastal zone, depth-integrated models are often employed. In a depth-integrated simulation, the properties of the bed can be parameterized into friction and roughness coefficients. Most often, the flow is a combination of waves and currents, and the bed is covered with ripples, which complicates the situation drastically. A large amount of attention has been devoted to specify the friction under these circumstances (Mathiesen and Madsen, 1996; Fredsøe et al., 1999). In the case of waves approaching the coast at an angle different from 90°, a long shore current is driven by the dissipation of wave energy. The situation is, therefore, one where the waves and the current are neither parallel nor perpendicular to one another, and the interaction between the two is very nontrivial. For a flat bed, Davies et al. (1988) showed that the mean velocity profile veers in the vertical, such that the direction of the current near the bed is different from the one away from the bed. The case of a ripple-covered bed, being not right-angled with respect to an incident current, but without waves, was studied by Barrantes and Madsen (2000). In addition, here, the direction of the velocity varies in the vertical, rotating from being parallel to ripple crests close to the bottom to being directed along the incident flow far away from it. Even though the mechanisms are different, in both cases, the orientation of the friction is different from that of the mean current. In the case of a pure wave motion and moderate shear stresses, the bed is covered by vortex ripples, which are mostly regular with long

* Corresponding author.
E-mail addresses: ken@isva.dtu.dk (K.H. Andersen), faraci@ingegneria.unime.it (C. Faraci).

0378-3839/02/$ - see front matter © 2002 Elsevier Science B.V. All rights reserved.
doi: 10.1016/S0378-3839(02)00158-8

straight crests, even though modulations can occur (Hansen et al., 2001). When a perpendicular current is added, the ripple crests show a sinusoidal variation, which was dubbed “serpentine ripples” by Lee Young and Sleath (1990). In such a case, Khelifa and Ouellet (2000) performed a laboratory investigation on ripples generated by a combined wave plus current flow, deriving empirical formulae in order to predict ripple characteristics.

The aim of the present work is to investigate the flow over a rippled bed in a wave plus current environment, accounting for a current coming at an arbitrary angle. An experimental investigation was performed in order to find the limits beyond which ripples cannot be considered regular and long-crested. Numerical simulations of the flow over a rippled bed were performed and the friction coefficient due to the combined wave plus current flow was estimated.

2. Experiments

The experiments were carried out in a 15×25-m basin where both waves and current could be generated. The water depth was varied between 0.4 and 0.45 m. In this range, it was possible to achieve reasonable wave and current velocities. In Fig. 1, a sketch of the basin, with the wave generators and absorbers placed along the sides parallel to the current flow, is reported.

The bed of the basin was made up with concrete, and in the middle area, a pit with a surface of 3.5×5.5 m was filled with sand, characterized by a median grain size equal to 0.18 mm. Waves were generated with piston-type wave makers, controlled by a computer. The latter reproduced Stokes waves with an imposed wave period and wave height. In order to create a current inside the basin, the water was forced to recirculate in the basin through a variable pump. The standard configuration, with an angle of incidence between the waves and the current of 90° was employed to carry out the present experimental investigation. Velocities were measured with a 300-mW, two-component DANTEC Laser Doppler Anemometer (LDA). Burst spectrum analyzers (BSA) were employed instead of frequency trackers due to the weak signal/noise ratio. The bed pattern was photographed with a digital camera. The pictures

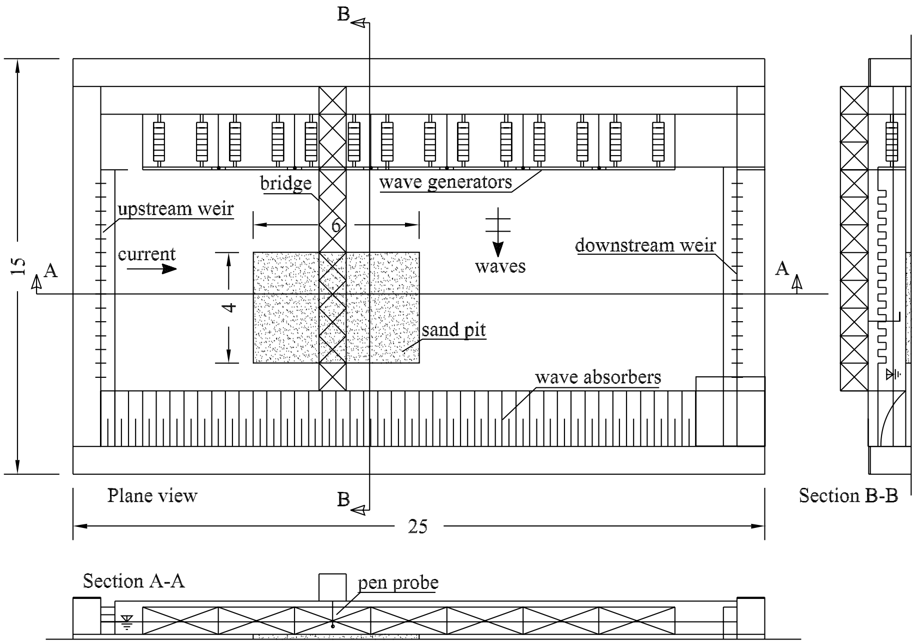

Fig. 1. Sketch of the basin.

of the sandy bottom were taken in the same area where the velocity measurements were acquired.

2.1. Experimental results

The test conditions are reported in Table 1. For each experiment, the adopted water depth D and the wave height H are reported. The wave period, T, was 1.1 s for all the tests. The ratio between the wave orbital velocity, U_w, and current velocity, U_c, were changed in the experiments. On the basis of the velocity time series taken at 0.04 m above the bed, an asymmetry index was defined. The asymmetry index is the ratio between the maximum velocities in the positive and negative half-periods, once the mean velocity have been subtracted. For wave heights smaller than 0.06 m (as in test no. 10), the calculated wave Shields parameter was found to be below the threshold needed to generate wave ripples, i.e., $\theta' \approx 0.045$. All the experiments were carried out adopting the standard configuration, that is, with an angle between the waves and the current equal to 90°. Such information is also reported in the Table 1.

The Shields parameter is defined as:

$$\theta' = \frac{U_f^2}{(s-1)gd} \tag{1}$$

where s is the relative density, $s=\rho_s/\rho$ (ρ_s and ρ being, respectively, the sediment and the water density), g is the acceleration due to gravity, d is the median grain size and U_f is the wave friction velocity. $U_f = \sqrt{\tau'/\rho\tau'}$ is the maximum shear stress on a flat bed during a wave period: $\tau'=(1/2)\rho f_w U_w^2$. The estimate of the friction coefficient f_w was carried

Table 1
Test conditions for the performed experiments

Test no.	Water depth, D (m)	Wave height, H (m)	Wave orbital velocity, U_w (m/s)	Current velocity, U_c (m/s)	Asymmetry index	Current direction, α_u (°)	Friction velocity (m/s)
1	0.40	0.10	0.19	0.09	0.81	90	0.018
2	0.40	0.12	0.24	0.08	0.72	90	0.022
3	0.40	0.12	0.26	0.17	0.70	90	0.023
4	0.40	0.12	0.30	0.22	0.54	90	0.026
5	0.40	0.12	0.32	0.24	0.60	90	0.027
6	0.40	0.10	0.27	0.23	0.61	90	0.024
7	0.40	0.08	0.21	0.24	0.58	90	0.020
8	0.40	0.06	0.16	0.24	0.65	90	0.016
9	0.40	0.06	0.15	0.24	0.66	90	0.016
10	0.40	0.04	0.10	0.21	0.87	90	0.012
11	0.40	0.10	0.21	0.06	0.82	90	0.020
12	0.40	0.12	0.24	0.05	0.83	90	0.022
13	0.40	0.08	0.18	0.06	0.72	90	0.018
14	0.40	0.12	0.26	0.07	0.86	90	0.023
15	0.40	0.10	0.22	0.10	0.84	90	0.020
16	0.40	0.10	0.20	0.13	0.77	90	0.019
17	0.45	0.10	0.20	0.14	0.97	90	0.019
18	0.45	0.11	0.22	0.14	0.95	90	0.020
19	0.45	0.12	0.22	0.15	0.94	90	0.021
20	0.45	0.10	0.20	0.14	0.94	90	0.019
21	0.45	0.12	0.23	0.12	0.96	90	0.021
22	0.45	0.10	0.19	0.18	0.80	90	0.018
23	0.45	0.12	0.21	0.22	0.98	90	0.020
24	0.45	0.12	0.21	0.20	0.95	90	0.016
25	0.45	0.10	0.16	0.18	0.95	90	0.016
26	0.45	0.12	0.21	0.19	0.90	90	0.020
27	0.45	0.11	0.21	0.16	0.93	90	0.020
28	0.45	0.12	0.23	0.03	0.95	90	0.015

out through the rough turbulent flow formula (Nielsen, 1992):

$$f_w = \exp\left[5.5\left(\frac{k_N}{a}\right)^{0.2} - 6.3\right] \quad (2)$$

where k_N is the Nikuradse equivalent roughness, equal to $2.5d$ and a is the wave orbital amplitude, $a = U_w/\omega$, ω being the wave angular frequency, $\omega = 2\pi/T$. The friction velocity is reported in the last column in Table 1.

The ratio between the current strength and the wave orbital velocity, U_c/U_w, was varied between 0.2 and 1.5. With the adopted experimental setup, it was not possible to obtain higher ratios: indeed an attempt to increase the ratio up to 2 was made in test no. 10, but as previously mentioned, the corresponding wave Shields parameter was found to be lower than 0.045. Hence, wave ripples could not develop and the pattern was mainly influenced by the current.

Different types of ripple patterns were observed when the velocity ratio U_c/U_w was changed. In order to take into account the response of the bed through the Shields parameter, the variability of the patterns with U_c/U_f was also considered.

Some general lines of behavior can be drawn. When the current is weak—the velocity ratio U_c/U_w is lower than 0.2 and the friction velocity ratio U_c/U_f is lower than 2—the ripples are not influenced by the presence of the current. The resulting pattern is a wave-dominated pattern, pretty regular and oriented normally to the wave propagation direction, not different from what is generally seen when currents are not superimposed (Fig. 2a). Some differences start to appear when the velocity ratio U_c/U_w exceeds 0.2 and the friction velocity ratio U_c/U_f is higher than 2. As in Fig. 2b, the ripple pattern shows the typical serpentine morphology which was also described by Lee Young and Sleath (1990), that is completely developed for a velocity ratio between 0.3 and 0.6, or the friction

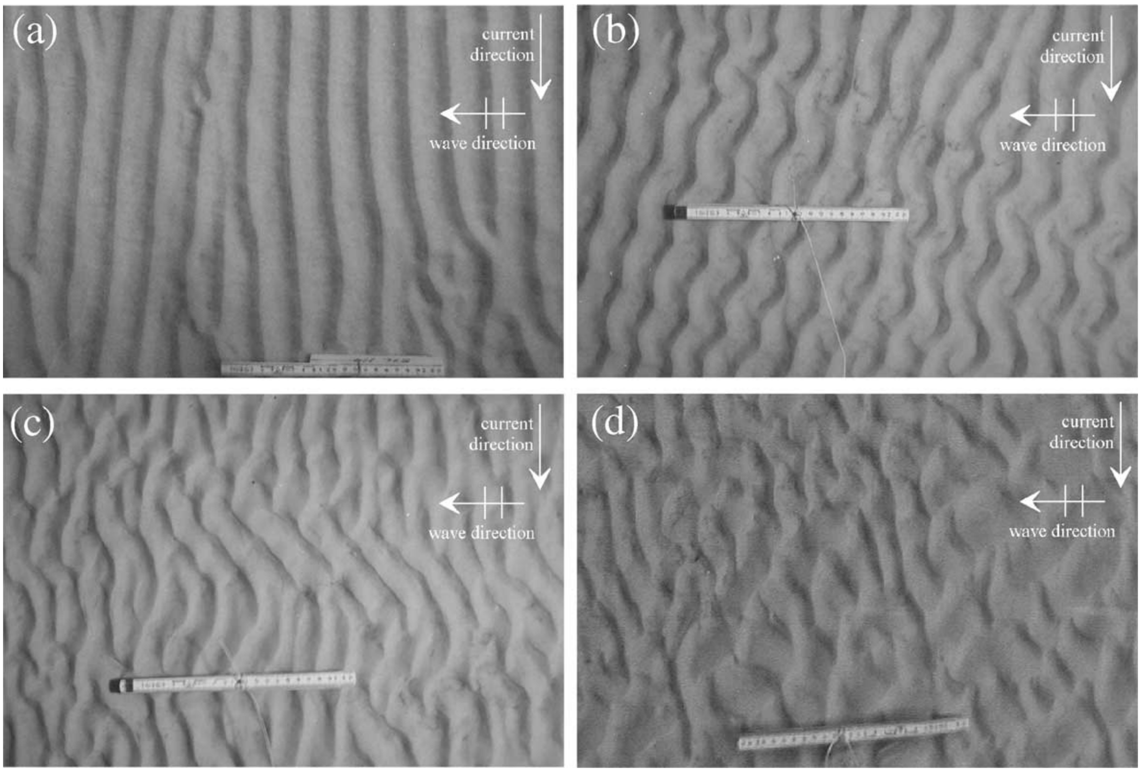

Fig. 2. Different types of ripple patterns: (a) regular (test no. 28, $U_c/U_w = 0.13$); (b) serpentine (test no. 21, $U_c/U_w = 0.5$); (c) segmented (test no. 22, $U_c/U_w = 0.9$); (d) irregular (test no. 8, $U_c/U_w = 1.5$). The size of the ruler is 20 cm.

velocity ratio between 3 and 6. The appearance of this pattern must be due to a instability of the vortex due to the interaction of the current parallel to the axis of the vortex.

At U_c/U_w around 0.6, a transitional phenomenon takes place: the current, becoming stronger, tries to break the ripple edges and makes the ripples pattern irregular. For a velocity ratio equal to 0.65 up to about 1.1, the ripple patterns appears pretty irregular, no longer characterized by a continuous line, but by small segments, that frequently interrupt and restart or merge together. The asymmetry in the strength of the lee vortices in each half-cycle is more evident as far as the current increases. Once the vortex is ejected, it is carried downstream by the current, eventually breaking the crest line. With the increase of the current velocity, the effects become more and more evident, and close to $U_c/U_w = 1.0-1.1$, the effects of the current appear also in the ripple marks and the ripples are characterized by an asymmetric profile like in the current ripples; in such case, the friction velocity ratio U_c/U_f ranges from 6 up to 11 (Fig. 2c).

Finally, for U_c/U_w higher than 1.1 (up to 1.5 in the present investigation) and friction velocity ratios greater than 11, the tendency to become more segmented is strongly enhanced. The final result looks like current ripples still coexist with small residual segmented ripples originally due to waves, thus, creating small sand streaks or spots (Fig. 2d).

Summarizing, it has been found that ripples are not affected by the presence of the superimposed current until the latter reach 20% of the wave orbital velocity. The ripple patches cease to be regular and long-crested when the velocity ratio reaches values of about 0.65. Nevertheless, up to velocity ratios equal to about 1.1, even though they assume a characteristic segmented feature, the ripples maintain a common orientation is small areas. The friction velocity ratio U_c/U_f was found to have the same trend as the velocity ratio U_c/U_w, that is, it tends to increase as the pattern irregularity increases. In what follows, the velocity ratio U_c/U_w has been chosen as the key parameter.

3. Numerical model

The large-scale flow over ripples in waves plus current is three-dimensional, except in the case where the waves and currents are in the same direction, as in Fredsøe et al. (1999). However, as previously seen, for low currents, the ripples are straight-crested in the z-direction. This basically means that all derivatives in the z-direction are zero, and the Reynolds-averaged Navier–Stokes equations can be written as (Jensen et al., 1999):

$$\frac{\partial u}{\partial t} + u\frac{\partial u}{\partial x} + v\frac{\partial u}{\partial y} = -\frac{1}{\rho}\frac{\partial p}{\partial x} + D(u) \tag{3}$$

$$\frac{\partial v}{\partial t} + u\frac{\partial v}{\partial x} + v\frac{\partial v}{\partial y} = -\frac{1}{\rho}\frac{\partial p}{\partial y} + D(v) \tag{4}$$

$$\frac{\partial w}{\partial t} + u\frac{\partial w}{\partial x} + v\frac{\partial w}{\partial y} = -\frac{1}{\rho}\frac{\partial p}{\partial z} + D(w) \tag{5}$$

where D is the diffusion operator:

$$D(\phi) = \frac{\partial}{\partial x}\left(\nu_T\frac{\partial \phi}{\partial x}\right) + \frac{\partial}{\partial y}\left(\nu_T\frac{\partial \phi}{\partial y}\right) \tag{6}$$

and ν_T is the turbulent diffusion.

The velocity in the z-direction is basically advected by the u and v velocities, and the only coupling between the flow in the z-direction (w) and the two other directions occurs through the contribution to ν_T. This means that w can be found by solving that equation on the 2d grid together with the equations for u and v and the continuity equation for the pressure. The eddy viscosity is calculated using a standard $k-\omega$ turbulence model (again assuming uniformity in the z-direction) (Wilcox, 1988):

$$\begin{aligned}\frac{\partial k}{\partial t} &+ u\frac{\partial k}{\partial x} + v\frac{\partial k}{\partial y}\\ &= \frac{\partial}{\partial x}\left(\nu + \sigma^*\nu_T\frac{\partial k}{\partial x}\right) + \frac{\partial}{\partial y}\left(\nu + \sigma^*\nu_T\frac{\partial k}{\partial y}\right)\\ &\quad + \nu_T\left[2\left(\frac{\partial u}{\partial x}\right)^2 + 2\left(\frac{\partial v}{\partial x}\right)^2 + \left(\frac{\partial u}{\partial y} + \frac{\partial v}{\partial x}\right)^2\right.\\ &\quad \left. + \left(\frac{\partial w}{\partial x}\right)^2 + \left(\frac{\partial w}{\partial y}\right)^2\right] - \beta^* k\omega \end{aligned} \tag{7}$$

$$\frac{\partial\omega}{\partial t}+u\frac{\partial\omega}{\partial x}+v\frac{\partial\omega}{\partial y} = \frac{\partial}{\partial x}\left(v+\sigma^* v_T\frac{\partial\omega}{\partial x}\right)+\frac{\partial}{\partial y}\left(v+\sigma^* v_T\frac{\partial\omega}{\partial y}\right) - \gamma v_T\frac{\omega}{k}\left[2\left(\frac{\partial u}{\partial x}\right)^2+2\left(\frac{\partial v}{\partial x}\right)^2+\left(\frac{\partial u}{\partial y}+\frac{\partial v}{\partial x}\right)^2 + \left(\frac{\partial w}{\partial x}\right)^2+\left(\frac{\partial w}{\partial y}\right)^2\right]-\beta\omega^2 \quad (8)$$

where

$$v_T=\gamma^*\frac{k}{\omega} \quad (9)$$

with standard closure coefficients as given by Wilcox (1988).

The flow is solved using a third-order ISNAS scheme in space (Zijlema, 1996) and first-order implicit in time. The grid is curvilinear and, thus, fitted to the bottom contours. The computational domain includes one ripple with periodic lateral boundary conditions, such that the computation is in fact taking place on an infinite train of equal ripples. For more details about the computational model, grid convergence tests, etc., see Tjerry (1995), Andersen (1999) and Jensen et al. (1999).

The oscillatory motion is perpendicular to the crests of the ripples, and is driven by an oscillating volume force. The current can come from an arbitrary angle (not only 90° as in the experiments), and is driven by a constant volume force (see Fig. 3). This volume force can be thought of as a hydrostatic pressure gradient.

In a combined wave and current flow with the current coming from an angle not parallel or orthogonal to the waves, the direction of the force needed to drive the steady current α_p (or the direction of the friction on the bed) will not be in the same direction as the current itself α_u. For a flat bed, this deviation can be up to 15° (Davies et al., 1988), but for a rippled bed, one can expect even larger deviations. Barrantes and Madsen (2000) measured deflections of the velocity vector toward ripple crest up to 55° with respect to the incident flow direction due to the presence of a drag component in the transverse direction, which turns the near bottom flow.

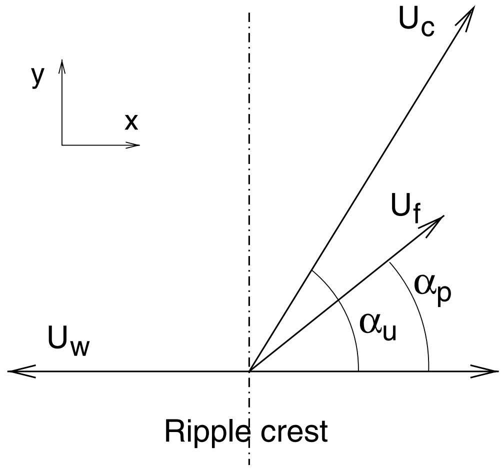

Fig. 3. Definition of the angles and directions. U_w is the amplitude of the oscillating flow, which is perpendicular to the ripple crests (dashed line). α_u is the angle of the steady current part (averaged over the wave period and over the ripple) and α_p is the direction of the friction.

There are two possibilities for setting the angle of the steady part of the current. Either the angle of the space- and time-averaged velocity can be fixed, or the angle of the volume force can be fixed. In the following simulations, the ratio U_c/U_w between the depth-averaged current strength and the wave orbital velocity was set. It was chosen to fix the depth-averaged angle of the incident current α_u, while the averaged direction of the drag α_p was found as a function of α_u.

4. Results

In all the runs, the size of the grid is 40 × 30, and the bed roughness caused by the sand grains is set to $k_N = 4.5 \times 10^{-4} D$, where D is the depth. A "basic" situation has been chosen, which corresponds to typical ripples found in the coastal zone. The ripples are assumed to be triangular; however, at the lower 20% of the ripple, a spline has been fitted to make the trough round. A triangular ripple with rounded troughs, fitted by a parabolic profile, was chosen to describe the bottom geometry. The length of the ripples is $\lambda = 1.2a$, where a is the amplitude of the orbital motion, the height is $h = 0.18\lambda$ and the depth (which has been arbitrarily chosen) is $D = 117h = 21a$.

4.1. Flow

The flow over the ripples is analysed as being a current-only flow averaged over space (one ripple) and time (the wave period). Close to the ripples, the wave part will dominate and create an effective enhanced roughness and friction which is felt by the average current.

In Fig. 4, four snapshots of the flow during one wave period are reported. The ratio between the current velocity and the maximum wave related velocity is $U_c/U_w = 1.0$ and the current comes at an angle of 45°. Even though the current is quite strong compared to the wave motion, two almost equally sized vortices are created in each half-wave period. On the top of each snapshot, the current seems to dominate, and it is stronger in the first half than in the second half.

In Fig. 5, space and time averages of the flow are shown. The error bars show the maximum and the minimum value of all the values entering the space and time average for a given y, i.e., $\max(\langle |u(x,y,t)| \rangle_{x,t})$ and $\min(\langle |u(x,y,t)| \rangle_{x,t})$, where $\langle \cdot \rangle_{x,t}$ is an average over the wave period and over x. For $y > 5h$, the variation vanishes, which means that above this height, the only motion is the oscillation induced by the waves. The size of the wave boundary layer is, therefore, $\delta_{bl} \approx 5h$. Above the boundary layer, a clear logarithmic layer is developed. The line shown is not a fit of the logarithmic layer, but it is drawn using the calculated shear stress on the bed, and the roughness k_N is found using Nikuradse's resistance formula (Schlichting, 1979):

$$\frac{\langle U \rangle}{\langle U_f \rangle} = 2.46 \ln\left(\frac{14.8D}{k_N}\right), \tag{10}$$

where the angular brackets denote average over space and time. The roughness found from this formula gives

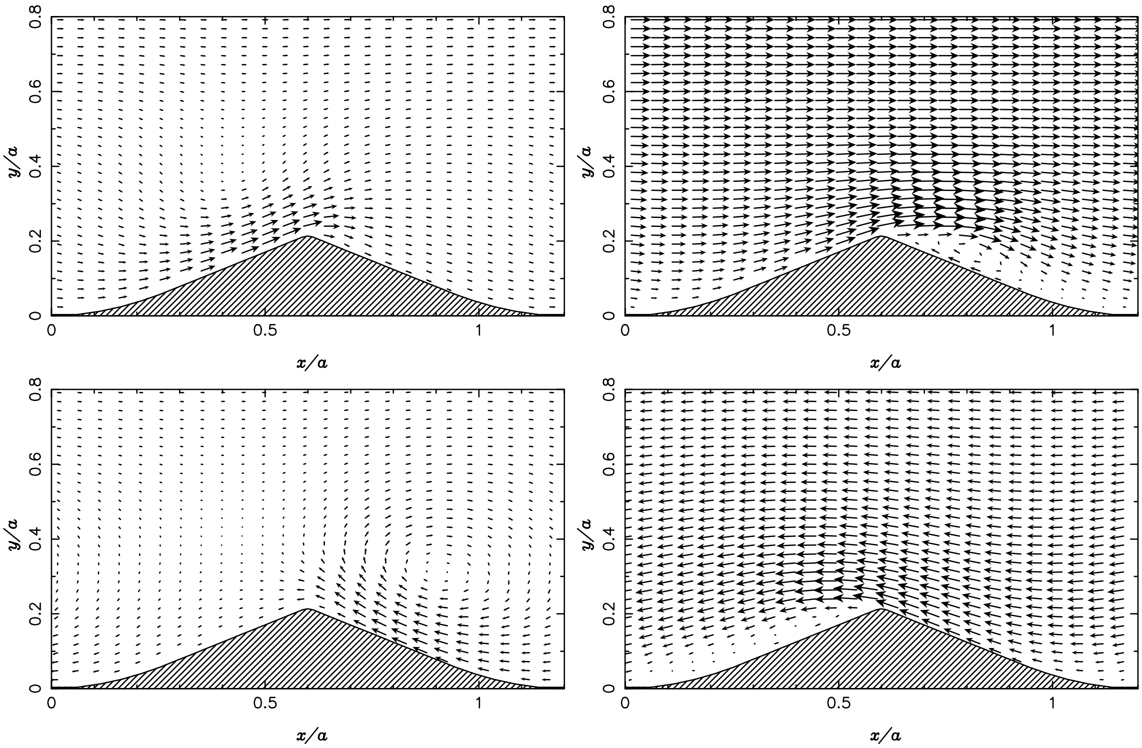

Fig. 4. Four snapshots of the u and v components of the flow over one ripple for the "standard" flow case: $D/h = 100$, $h/\lambda = 0.18$, $\lambda/a = 1.2$, $U_c/U_w = 1.0$ and $\alpha_u = 45°$.

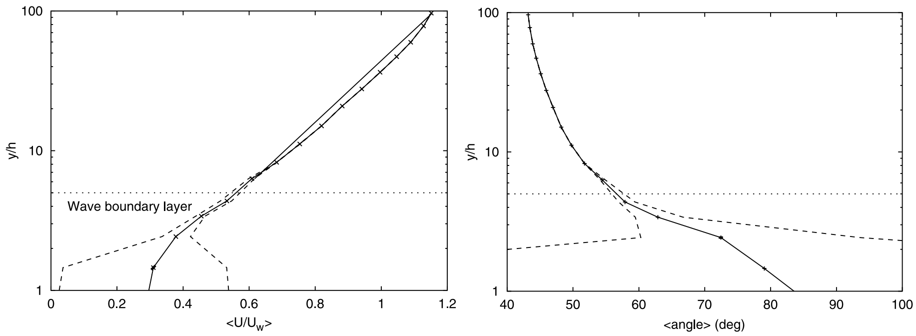

Fig. 5. The flow over the ripples averaged over the ripple and over one wave period (left). The dashed lines represents the maximum and minimum velocities occurring at the given point in y. Right: the variation of the flow angle with z. The conditions are the same as in Fig. 4.

$k_N = 8.2h$ which is a bit overpredicted. The real roughness found from fitting to the profile is $k_N = 6.8h$.

Well above the boundary layer, the flow has almost the direction in which it is forced, i.e., 45° in this case (Fig. 5b). However, close to the bed, the average current changes direction such that it tends to align parallel to the ripple crest (90°). A similar change of flow angle with y is also observed over a flat bed (Davies et al., 1988), but there the effect is due to the nonlinear relation between the current and the shear stress. This effect is, of course, also in play here, but in this case, the dominating part is the bed topography, which turns the flow parallel to the ripple crests.

4.2. Friction

The space- and time-averaged friction in the x-direction has been found from the driving pressure gradient as:

$$\tau_x = D\left\langle \frac{\partial p}{\partial x} \right\rangle \tag{11}$$

and similarly for the y-direction. D is the depth of the computational domain and the angular brackets denote average over space and time. The total friction is $\tau^2 = \tau_x^2 + \tau_y^2$, and the friction factor f_c is obtained from:

$$\tau = \frac{1}{2}\rho f_c \langle U \rangle^2 \tag{12}$$

In Fig. 6, the friction coefficient due to the combined waves plus current is plotted as a function of the angle of the current. The friction factor as generated by current alone (i.e., when the velocity ratio tends to infinity) is also shown in the same picture. The friction has been calculated for a slightly wider range of the velocity ratio than that strictly found from the experiments due to the fact that the Shields parameter corresponding to waves, for the tests realized with U_c/U_w higher than 1, was sensibly lower than the current one. Two trends are clear: (1) the smaller the current, the larger the friction, and (2) the friction decreases with the angle. The first trend is commonly known (Fredsøe et al., 1999), and simply stems from the fact that for small currents the effect of the waves dominates (for $\langle U \rangle \to 0$ the current friction diverges). The second trend is because the friction is larger when the current is perpendicular to a ripple (when $\alpha_u = 0°$) due to form drag experienced by the flow, than when it is parallel to the ripple ($\alpha_u = 90°$).

In Fig. 7, the friction is normalized by the current only friction factor f_{co}. Starting from Fredsøe et al. (1999), where the relative friction was described in terms of a single power law, independently of the wide range of the involved parameters, here the same power law structure has been adopted to explain the trend of the relative friction with the velocity ratio. The power law has the structure:

$$\frac{f_{wc}}{f_{co}} = A\left(\frac{U_c}{U_w}\right)^{-B} + 1 \tag{13}$$

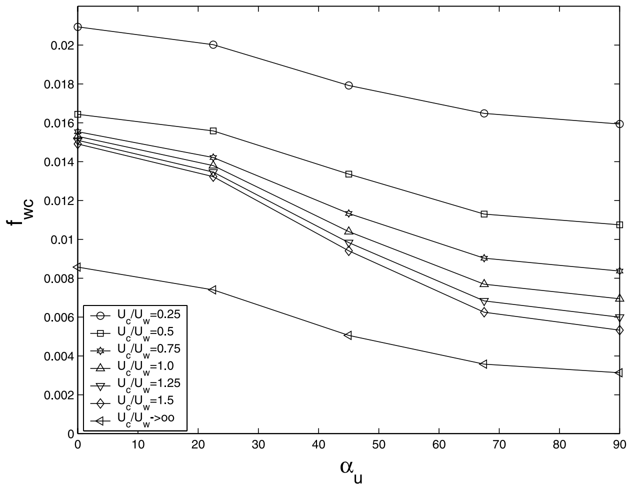

Fig. 6. The wave plus current friction due to combined wave plus current over the rippled bed as a function of the mean current direction α_u.

where the two coefficients A and B vary with the current angle and have been evaluated by means of a Boltzmann approximation to be:

$$A = \frac{-0.048}{1 + \exp\dfrac{\alpha_u - 36.9}{13.8}} + 1.23 \tag{14}$$

$$B = \frac{-0.495}{1 + \exp\dfrac{\alpha_u - 46.9}{12.2}} + 0.90 \tag{15}$$

In Eqs. (14) and (15), α_u is expressed in degrees.

As in Fredsøe et al. (1999), the wave plus current friction factor tends to the current only friction as the U_c/U_w ratio tends to infinity.

As expected, there is a difference between the angle of the flow and that of the friction (see Fig. 8). Basically, the friction prefer to be aligned parallel to the ripple crest, due, as explained by Barrantes and Madsen (2000), to the presence of a drag component in the transverse direction, which turns the near bottom flow toward ripple crests. At $\alpha_u = 90°$, there is no difference as the waves and the current are orthogonal. There is a little advance of the friction at the bed with

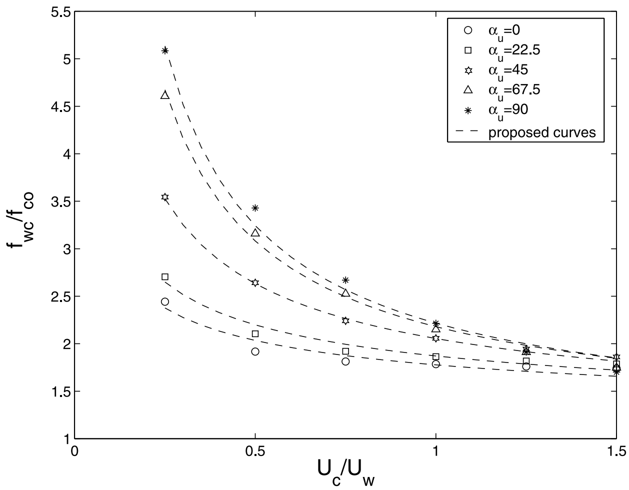

Fig. 7. The wave plus current friction normalize with the current-only friction as a function of the current strength.

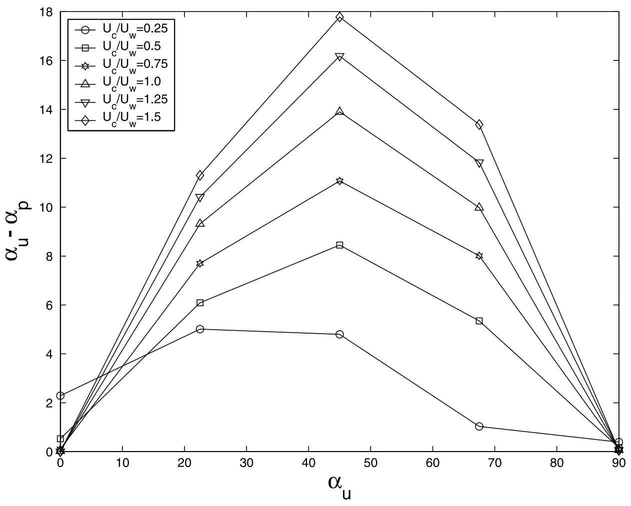

Fig. 8. Deviation of the direction of the bed friction $\alpha_u - \alpha_p$ compared to the current direction α_u.

respect to the current direction for $\alpha_u = 0°$ that immediately inverts the tendency already for $\alpha_u = 22.5°$. The maximum deviation between the two directions, as it is clearly visible from Fig. 8, occurs at $\alpha_u = 45°$.

5. Conclusion

An experimental investigation of ripple geometry was carried out in a combined wave plus current flow, in order to find the conditions for regular ripple formation. It was observed that ripple crests look like straight lines until the current is about 20% of the wave velocity. A waviness on the crest-line appears when the current is less than 60% of the orbital velocity, while as soon as the current and the wave orbital velocity reach approximately the same value, any regularity is broken. The numerical simulations were performed by choosing a case study representative of natural conditions and by changing the angle formed by the wave and the current direction.

The main results of the computations can be summarized in the following. For what concerns the flow:

1. in the presence of both waves and currents close to the rippled bed, the wave effects dominates over the current, enhancing the bottom roughness;
2. the roughness that was found from Nikuradse's formula predicts the roughness of the flow quite well;
3. close to the bed, the current is aligned parallel to the ripple crests.

For what concerns the friction:

1. the friction factor due to the combined flow decreases with the angle of the current;
2. the normalized friction factor f_{wc}/f_{co} increases when the current decrease; it can be expressed as a power law depending on the ratio U_c/U_w and parameterized in terms of the current angle, α_u, independently on ripple geometry;
3. the angle α_u formed by the current deviates from the direction of the friction, α_p, with a maximum deviation of 18° at $\alpha_u = 45°$. This is much more than that predicted for a flat bed Davies et al. (1988).

We emphasize that the experiments show that ripples are only long-crested up to a current of 0.65 times the orbital velocity. Thus, the results for higher current strengths are outside the range where we can expect the calculations to be valid.

It should be remembered that to use Eq. (13) to calculate the wave plus current friction factor, knowledge of the current-only friction factor, f_{co}, for the same current direction and for the same ripple geometry as the one in waves plus current is needed.

The third point related to the flow, namely, that the current prefer to be aligned parallel to the ripple crests, is potentially very important for sediment transport. The transport direction is governed by the direction of the current close the bed, rather than by the mean current. This consideration indicates that the transport will preferably be parallel to the ripple crests, i.e., orthogonal to the waves. Hence, in the presence of nonshore parallel ripples, the crest-aligned current close to the bed will have a component which is oriented away from the coast. As a consequence, the sediment transport will have a component directed away from the coast, and not only along it, as would be naively expected.

Acknowledgements

The present work has been carried out in partial fulfillment of C.F.'s doctoral degree.

References

Andersen, K., 1999. Ripples beneath surface waves and topics in shell models of turbulence. PhD thesis, Niels Bohr Institute, Copenhagen University. http://www.nbi.dk/~kenand/Thesis.html.

Barrantes, A.I., Madsen, O.S., 2000. Near bottom flow and flow resistance for currents obliquely incident to two dimensional roughness elements. J. Geophys. Res. 105 (C11), 26253–26264.

Davies, A., Soulsby, R., King, H., 1988. A numerical model of the combined wave and current bottom boundary layer. J. Geophys. Res. 93 (C1), 491–508.

Fredsøe, J., Andersen, K.H., Sumer, M., 1999. Wave plus current over a ripple-covered bed. Coast. Eng. 38, 177–221.

Hansen, J.L., van Hecke, M., Haaning, A., Ellegaard, C., Andersen, K.H., Bohr, T., Sams, T., 2001. Instabilities in sand ripples. Nature 410, 324.

Jensen, J., Madsen, E., Fredsøe, J., 1999. Oblique flow over dredged channels: I. Flow description. J. Hydraul. Eng. 125 (11), 1181–1190.

Khelifa, A., Ouellet, Y., 2000. Prediction of sand ripple geometry under waves and currents. J. Waterw. Port Coast. Ocean Eng. 126 (1), 14–22.

Lee Young, J., Sleath, J., 1990. Ripple formation in combined transdirectional steady and oscillatory flow. Sedimentology 37, 509–516.

Mathiesen, P.P., Madsen, O.S., 1996. Waves and current over a fixed ripples bed: 1. Bottom roughness experienced by currents in the presence of waves. J. Geophys. Res. 101 (C7), 16543–16550.

Nielsen, P., 1992. Coastal Bottom Boundary Layer and Related Topics. World Scientific, Singapore.

Schlichting, H., 1979. Boundary-Layer Theory. McGraw-Hill, New York.

Tjerry, S., 1995. Morphological calculation of dunes in alluvial rivers. PhD thesis, ISVA, The Danish Technical University.

Wilcox, D., 1988. Reassessment of the scale-determining equation for advanced turbulence models. AIAA J. 26 (11), 1299–1310.

Zijlema, M., 1996. On the construction of a third-order accurate monotone convection scheme with application to turbulent flows in general domains. Int. J. Numer. Methods Fluids 22, 619–641.